PHYSICAL REVIEW D **88,** 115006 (2013)

Charged Higgs production in association with $W^{\pm}$ at large hadron colliders

Guo-Li Liu,[1,3] Fei Wang,[1,3] and Shuo Yang[2,3]

[1]*Physics Department, Zhengzhou University, Henan 450001, China*
[2]*Physics Department, Dalian University, Dalian 116622, China*
[3]*Kavli Institute for Theoretical Physics China, Academia Sinica, Beijing 100190, China*

(Received 1 April 2013; published 3 December 2013)

Many new physics models beyond the standard model, such as the littlest Higgs models and the left-right twin Higgs models, predict the existence of the large charged Higgs couplings $H^- q\bar{b}$ and $H^+ b\bar{q}$, where $q = t$ or the new vectorlike heavy quark T. On the other hand, some new physics models, like the littlest Higgs, also predict the gauge-Higgs couplings. Such couplings may have rich collider phenomenology. We focus our attention on these couplings induced by the littlest Higgs models and the left-right twin Higgs models and consider their contributions to the production cross section for $W^{\pm}H^{\mp}$ production at the large hadron colliders. We find that the cross sections in the littlest Higgs models on the parton level $gg \to W^{\pm}H^{\mp}$ and $q\bar{q} \to W^{\pm}H^{\mp}$ ($q = u, d, s, c, b$) may reach tens of dozens femtobarns in reasonable parameter space at the collision energy of 14 TeV and that the total cross section can even reach a few hundred femtobarns in certain favored space. While in the left-right twin Higgs models, the production rates are basically one order lower than those in the littlest Higgs models. Therefore, due to the large cross sections of that in the littlest Higgs models, it may be possible to probe the charged Higgs via this process in a certain parameter space.

DOI: 10.1103/PhysRevD.88.115006 PACS numbers: 13.85.Lg, 12.60.Fr, 12.60.Cn

I. INTRODUCTION

The primary goal of the Large Hadron Collider (LHC) at CERN is to verify the electroweak symmetry breaking mechanism and to discover or rule out the existence of a Higgs boson. Since both the ATLAS and CMS collaborations discovered a Higgs bosonlike particle with mass of around 125 GeV at a significance of 5σ last year, the goal seems to have been reached [1,2]. Apart from searches for the Higgs boson, there is an ongoing hunt for signals of physics beyond the standard model (SM) at the LHC, and hopefully these experiments will shed some light on physics at the TeV scale.

Due to the incompletion, aesthetical and theoretical problems such as the famous hierarchy problem and triviality problem of the SM Higgs boson, various new physics models beyond the SM that try to solve in different ways the previously mentioned problems are proposed. For example, in the little Higgs (LH) [3] models, the Higgs bosons emerge as the pseudo Nambu-Goldstone bosons associated with the spontaneous breaking of a global symmetry. In order to implement the collective symmetry breaking mechanism, new particles such as heavy gauge bosons and top partners are introduced. Quadratically divergent corrections contributed by such new particles to the Higgs boson masses cancel out those induced by the top quark and gauge boson loops at the one-loop level. Thus, not much fine-tuning is needed in the LH model with a cutoff scale of $\mathcal{O}(10$ TeV).

Another example is the left-right twin Higgs (LRTH) [4] models. Again, the Higgs bosons in nature are pseudo Goldstone bosons from spontaneously broken global symmetry. The Higgs bosons obtain masses from the gauge and Yukawa interactions which break the global symmetry. As the left-right symmetry was imposed to the twin Higgs mechanism, the quadratic terms in the Higgs potential respect the global symmetry, and the contributions to the Higgs masses cancel out. The logarithmically divergent terms, however, are radiatively generated and are not invariant under global symmetry and contribute masses to the pesudo Goldstones. The resulting Higgs mass is in the field of the electroweak scale with the cutoff at about 5–10 TeV.

The LH models and the LRTH models predict multiplet physical Higgs bosons, two of which are charged ones. Since it is hard to distinguish between the CP-even Higgs bosons in such new physics models and the Higgs boson in the SM, any observation of a charged Higgs will be a crucial signature for new physics beyond the SM. That is why the charged scalar particles have attracted much attention in the previous years by different high energy physics experiments and theories, and they will certainly be probed at the LHC.

The search for Higgs bosons and new physics particles and the study of their properties are among the prime objectives of the LHC [5]. Since the discovery of the charged Higgs bosons will be the evidence of new physics beyond the SM, there are increasing interests in theoretical and experimental studies to provide the basis for its accurate exploration. Therefore, the LH and LRTH models are very interesting, since in these models charged scalars are predicted and they may possess larger tree-level or one-loop top or bottom Yukawa couplings, so we may detect the new Yukawa coupling in these models, which may serve as a sensitive probe of the two models.

Much effort is made for the search for charged Higgs bosons. From its exclusive decay modes $H^{\pm} \to \tau\nu$ and $H^{\pm} \to cs$, the LEP search experiments [6,7] have given a direct detection limit $M_{H^{\pm}} > 78.6$ GeV. With different mass range, the search approaches for charged Higgs bosons at the hadron collider are distinct. When the charged Higgs mass is low, the signal will be $t \to H^{+}b \to \bar{\tau}\nu_{\tau}b$. The Tevatron search is mainly focused on the low mass range $m_{H^{\pm}} < m_t$ due to phase space suppression for a heavy charged Higgs boson production and any signal of the charged Higgs has not been found, which means that the mass of the charged Higgs is larger than 160 GeV [8]. At the LHC, however, the charged Higgs search can be feasible via the $gb \to tH^{-}$ and $gg \to t\bar{b}H^{-}$ production up to a large mass range since the LHC collision energy is large [9]. When the charged Higgs is heavy $m_{H^{\pm}} > m_t$, the signal is from the main production process $gb \to tH^{-}$ and $gg \to t\bar{b}H^{-}$ followed by its main decay $H^{-} \to t\bar{b}$ [10,11].

Motivated by new technique of "jet substructure" [12–16] developed for highly boosted massive particles, a "hybrid-R reconstruction method," which can use the top tagging and the b tagging for other isolated b jets, as well as the full reconstructed objects in the final state to suppress the background, is proposed to investigate the full hadronical decay channel of the heavy charged Higgs production.

Recently, discussions on neutral or charged Higgs production at the LHC have been carried out, see, e.g., Refs. [17–23]. Both the LH and LRTH models predict neutral or charged (ϕ^0, $\phi^{\pm}$, or $H^{\pm}$) scalars with large Yukawa couplings to the third generation quarks in addition to a SM-like Higgs. They also predict one vectorlike heavy top quark T and new gauge bosons (A_H, Z_H, W_H). Such new particles can be regarded as typical features of those models. The signals of these two models have already been studied in the work environment of linear colliders and hadron-hadron colliders [24], but most of the attention has concentrated on the neutral scalars and new gauge bosons. Here we will discuss the single production of the charged scalars at the LHC.

For the production of a charged scalar in association with a W boson at the LHC, there are mainly two kinds of partonic subprocesses that contribute to the hadronic cross section $pp \to \phi^{\pm}W^{\mp}$: the $q\bar{q}$ ($q = u, d, c, s, b$) annihilation and the gg fusion. Processes like these have been studied; for example, in the minimal supersymmetric standard model, many studies have been conducted on the ϕW productions [25], and they may constraint our results. In this paper, to probe the littlest Higgs models and the left-right twin Higgs models, we shall discuss the production of the charged scalar $\phi^{\pm}$ in association with the SM gauge bosons $W^{\mp}$ via those two kinds of subprocesses.

This work is organized as follows. In Sec. II we recapitulate the LH models, give the couplings relevant to our calculation, and then discuss the numerical results. Similarly, in Sec. III the LRTH models are simply described and the numerical results are given. Finally, we compare the results predicted by the two models and give the conclusion in Sec. IV.

II. THE LH MODEL AND $W^{\pm}H^{\mp}$ PRODUCTION AT THE LHC

A. The LH model and the relative couplings

The littlest Higgs model [26] is based on the $SU(5)/SO(5)$ nonlinear sigma model. The global symmetry breaks from $SU(5)$ to $SO(5)$, generating 14 Goldstone bosons, and the gauge symmetry from $[SU(2) \times U(1)]^2$ to $SU(2) \times U(1)$, the SM electroweak gauge group. Four of these Goldstone bosons are eaten by the broken gauge generators, resulting in four massive gauge bosons A_H, Z_H, and $W_H^{\pm}$. The remaining ten states transform under the SM gauge group as a doublet H and a triplet Φ. The doublet vacuum expectation value (VEV) further breaks the gauge symmetry $SU(2) \times U(1)$ into $U(1)_Y$, eating three scalars of it and leaving only a CP-even Higgs, usually regarded as the SM Higgs, which has been discovered at the LHC [1,2].

When the fields rotate to the mass eigenstates, the gauge bosons mix by the mixing angles s and s',

$$s = \frac{g_2}{\sqrt{g_1^2 + g_2^2}}, \qquad s' = \frac{g_2'}{\sqrt{g_1'^2 + g_2'^2}}. \tag{1}$$

In the LH models [26], a new set of heavy vectorlike fermions $\tilde{t}$ and $\tilde{t^c}$ is introduced in order to cancel the top quark quadratic divergence, since they couple to the Higgs field. Choosing the Yukawa form of the coupling of the SM top quark to the pseudo Goldstone bosons and the heavy vector pair in the LH models, then diagonalizing the mass terms, one can straightforwardly work out the Higgs-quark interactions, as given in Ref. [26], and we list them in Table I for convenience.

The couplings (related to our calculation) of the new particles to the SM particles, which include (1) the three-point couplings of the gauge boson to the scalars, including case I (one gauge boson to two scalars) and case II (two gauge bosons and one scalar), (2) charged gauge boson-fermion couplings, and (3) the scalar-fermion couplings (which can be found in Ref. [26]) are extracted here as $P_L = (1 - \gamma^5)/2$ and $x_L \equiv \lambda_1^2/(\lambda_1^2 + \lambda_2^2)$, where λ_1, λ_2 are the Yukawa coupling of order $\mathcal{O}(1)$. The neutral gauge boson-fermion couplings can also be extracted as those in Table II [26].

B. The LH ϕW associated production at the LHC

At the LHC, the parton level cross sections are calculated at the leading order as

$$\hat{\sigma}(\hat{s}) = \int_{\hat{t}_{\min}}^{\hat{t}_{\max}} \frac{1}{16\pi\hat{s}^2} \bar{\Sigma}|M_{\text{ren}}|^2 d\hat{t}, \tag{2}$$

TABLE I. The three-point couplings of the gauge boson, the scalars, and the fermions in the littlest Higgs models. The momenta are taken as $V_\mu S_1(p_1)S_2(p_2)$, and the particles are in the mass eigenstates with the momenta outgoing.

Particles	Vertices	Particles	Vertices
$W^+_{L\mu}H\Phi^-$	$-\frac{ig}{2}(\sqrt{2}s_0 - s_+)(p_1 - p_2)_\mu$	$W^+_{L\mu}A_{H\nu}\Phi^-$	$-\frac{i}{2}gg'\frac{(c'^2-s'^2)}{2s'c'}(vs_+ - 4v')g_{\mu\nu}$
$W^+_{L\mu}\Phi^0\Phi^-$	$-\frac{ig}{\sqrt{2}}(p_1 - p_2)_\mu$	$W^+_{L\mu}Z_{L\nu}\Phi^-$	$-i\frac{g^2}{c_w}v'g_{\mu\nu}$
$W^+_{L\mu}\Phi^P\Phi^-$	$\frac{g}{\sqrt{2}}(p_1 - p_2)_\mu$	$W^+_{L\mu}Z_{H\nu}\Phi^-$	$ig^2\frac{(c^2-s^2)}{2sc}v'g_{\mu\nu}$
$W^{+\mu}_L\bar{t}_Lb_L$	$\frac{ig}{\sqrt{2}}[1 - \frac{v^2}{f^2}(\frac{1}{2}x_L^2 + \frac{1}{2}c^2(c^2 - s^2))]\gamma^\mu V^{\rm SM}_{tb}P_L$	$W^{+\mu}_L\bar{T}_Lb_L$	$\frac{g}{\sqrt{2}}\frac{v}{f}x_L\gamma^\mu V^{\rm SM}_{tb}P_L$
$H\bar{t}t$	$-i\frac{m_t}{v}[1 - \frac{1}{2}s_0^2 + \frac{v}{f}\frac{s_0}{\sqrt{2}} - \frac{2v^2}{3f^2} + \frac{v^2}{f^2}\frac{\lambda_1^2}{\lambda_1^2+\lambda_2^2}(1 + \frac{\lambda_1^2}{\lambda_1^2+\lambda_2^2})]$	$H\bar{T}T$	$-i\frac{\lambda_1^2}{\sqrt{\lambda_1^2+\lambda_2^2}}(1 + \frac{\lambda_1^2}{\lambda_1^2+\lambda_2^2})\frac{v}{f}$
$\Phi^0\bar{t}t$	$-\frac{im_t}{\sqrt{2}v}(\frac{v}{f} - \sqrt{2}s_0)$	$\Phi^P\bar{t}t$	$-\frac{m_t}{\sqrt{2}v}(\frac{v}{f} - \sqrt{2}s_P)\gamma^5$
$\Phi^+\bar{t}b$	$-\frac{i}{\sqrt{2}v}(m_tP_L + m_bP_R)(\frac{v}{f} - 2s_+)$	$\Phi^+\bar{T}b$	$-\frac{im_t}{\sqrt{2}v}(\frac{v}{f} - 2s_+)\frac{\lambda_1}{\lambda_2}P_L$

TABLE II. Neutral gauge boson-fermion couplings and $y_u = -2/5$ and $y_e = 3/5$ are required by the anomaly cancellation. The couplings are given in the form $i\gamma^\mu(g_V + g_A\gamma^5)$.

Particles	g_V	g_A
$Z_L\bar{u}u$	$-\frac{g}{2c_w}\{(\frac{1}{2} - \frac{4}{3}s_w^2) - \frac{v^2}{f^2}[c_wx_Z^{W'}c/2s + \frac{s_wx_Z^{B'}}{s'c'}(2y_u + \frac{7}{15} - \frac{1}{6}c'^2)]\}$	$-\frac{g}{2c_w}\{-\frac{1}{2} - \frac{v^2}{f^2}[-c_wx_Z^{W'}c/2s + \frac{s_wx_Z^{B'}}{s'c'}(\frac{1}{5} - \frac{1}{2}c'^2)]\}$
$Z_L\bar{d}d$	$-\frac{g}{2c_w}\{(-\frac{1}{2} + \frac{2}{3}s_w^2) - \frac{v^2}{f^2}[-c_wx_Z^{W'}c/2s + \frac{s_wx_Z^{B'}}{s'c'}(2y_u + \frac{11}{15} + \frac{1}{6}c'^2)]\}$	$-\frac{g}{2c_w}\{\frac{1}{2} - \frac{v^2}{f^2}[c_wx_Z^{W'}c/2s + \frac{s_wx_Z^{B'}}{s'c'}(-\frac{1}{5} + \frac{1}{2}c'^2)]\}$
$A_H\bar{u}u$	$\frac{g'}{2s'c'}(2y_u + \frac{17}{15} - \frac{5}{6}c'^2)$	$\frac{g'}{2s'c'}(\frac{1}{5} - \frac{1}{2}c'^2)$
$A_H\bar{d}d$	$\frac{g'}{2s'c'}(2y_u + \frac{11}{15} + \frac{1}{6}c'^2)$	$\frac{g'}{2s'c'}(-\frac{1}{5} + \frac{1}{2}c'^2)$
$Z_H\bar{u}u$	$gc/4s$	$-gc/4s$
$Z_H\bar{d}d$	$-gc/4s$	$gc/4s$

with

$$\hat{t}_{\max,\min} = \frac{1}{2}\Big\{m_{p_1}^2 + m_{p_2}^2 - \hat{s} \pm \sqrt{[\hat{s} - (m_{p_1} + m_{p_2})^2][\hat{s} - (m_{p_1} - m_{p_2})^2]}\Big\}, \tag{3}$$

where p_1 and p_2 are the first and second initial particles in the parton level, respectively. For our case, they could be gluon g and quarks u, d, c, s, b, etc.

The total hadronic cross section for $pp \to SS' + X$ can be obtained by folding the subprocess cross section $\hat{\sigma}$ with the parton luminosity

$$\sigma(s) = \int_{\tau_0}^1 d\tau \frac{dL}{d\tau}\hat{\sigma}(\hat{s} = s\tau), \tag{4}$$

where $\tau_0 = (m_{p_1} + m_{p_2})^2/s$, and s is the pp center-of-mass energy squared. $dL/d\tau$ is the parton luminosity given by

$$\frac{dL}{d\tau} = \int_\tau^1 \frac{dx}{x}[f^p_{p_1}(x, Q)f^p_{p_2}(\tau/x, Q) + (p_1 \leftrightarrow p_2)], \tag{5}$$

where $f^p_{p_1}$ and $f^p_{p_2}$ are the parton p_1 and p_2 distribution functions in a proton, respectively. In our numerical calculation, the CTEQ6L parton distribution function is used [27] and we take the factorization scale Q and the renormalization scale μ_F as $Q = \mu_F = m_\phi + m_W$. The loop integrals are evaluated by the LoopTools package [28].

As for the SM parameters, throughout this paper, we take $m_t = 173$ GeV [29], $m_W = 80.38$ GeV, $m_Z = 91.19$ GeV, and $G_F = 1.16637 \times 10^{-5}$ GeV^{-2} [30], $\alpha_s(m_Z) = 0.118$, and neglect the bottom quark mass as well as other light quark masses.

Now we discuss the main LH parameters involved.

(1) New scalar masses: charged pseudoboson, neutral bosons, and the SM-like Higgs. The SM-like Higgs was discussed after the CERN experiment data release in, e.g., Refs. [31,32], and the discussions showed that the LH models may survive when $f \geq 800$ GeV. Here we choose the loose constraints that $f \geq 500$ GeV and the SM-like Higgs mass as the current experiment value: 125 GeV [1,2]. The masses of other scalars m_ϕ, despite the small electromagnetic difference, are the same and their constraints are quite loose. Here we take m_ϕ as a free parameter varying from 200 to 600 GeV, according to Refs. [6,7,10,11,33].

(2) The mixing parameters s, c, and s', c' in the range of 0–1. Here we will take, however, s free parameters from 0–0.5, and take $s' = 0.5$ so $c' > 0.62$ according to Refs. [34,35].

(3) As for the scale f, one can have a rough estimate of the natural scale [26]

$$f \leq \frac{4\pi m_H}{\sqrt{0.1 a_{\max}}} \simeq \frac{8\ \text{TeV}}{\sqrt{a_{\max}}}\left(\frac{m_H}{200\ \text{GeV}}\right), \quad (6)$$

where $a_{\max}$ denotes the largest coefficient which could be of the order of 10. So for a light m_H, f may have a lower upper limit.
Here we also estimate f in some particular situation, such as that shown in Refs. [35,36] in which the $U(1)$ sector can be modified by adding an additional $U(1)$ and only gauging $U(1)_Y$, in the $SU(6)/SP(6)$ realization. This may bring f to survive in the area of less than 1 TeV. In our calculation, we will weaken the constraints a little and take $500 < f < 2000$ GeV.

(4) Regarding the new gauge boson masses, the charged and neutral gauge bosons' final masses related to our calculation are written as [26]

$$M^2_{W_L^\pm} = m_w^2\left[1 - \frac{v^2}{f^2}\left(\frac{1}{6} + \frac{1}{4}(c^2 - s^2)^2\right) + 4\frac{v'^2}{v^2}\right], \quad (7)$$

$$M^2_{Z_L} = m_z^2\left[1 - \frac{v^2}{f^2}\left(\frac{1}{6} + \frac{1}{4}(c^2 - s^2)^2 + \frac{5}{4}(c'^2 - s'^2)^2\right) + 8\frac{v'^2}{v^2}\right], \quad (8)$$

$$M^2_{A_H} = m_z^2 s_w^2\left(\frac{f^2}{5 s'^2 c'^2 v^2} - 1 + \frac{x_H c_w^2}{4 s^2 c^2 s_w^2}\right), \quad (9)$$

$$M^2_{Z_H} = m_w^2\left(\frac{f^2}{s^2 c^2 v^2} - 1 - \frac{x_H s_w^2}{s'^2 c'^2 c_w^2}\right), \quad (10)$$

where $m_z \equiv gv/(2c_w)$ and $m_w = m_z c_w$ are the SM neutral and charged boson mass, and the x_H can be found in Ref. [26]. The masses of the Z_H, however, are still constrained by the LHC experiments. For example, the ATLAS [37,38] and CMS collaborations [39,40] have detected the heavy vector boson as a dijet resonance and give the lower limits of the bosons, i.e., $M_{Z_H} > 1.62$ TeV, which bound the limits of the parameter involved. Since the last term of the M_{Z_H} in Eq. (10) is very small, the first term decides the relation of the parameters f and s; that is, the parameters f and s are restricted by each other when the Z_H mass range is set. We show in Fig. 1 the contour of the two parameters given the lower limit of the new heavy neutral mass M_{Z_H}.

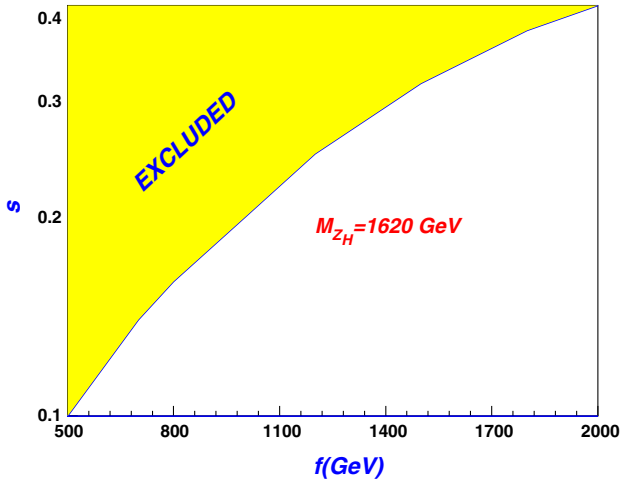

FIG. 1 (color online). In the LH, the contour of the parameters f and s for the lower limit of the new heavy gauge boson mass $M_{Z_H} = 1620$ TeV.

From Fig. 1, we can see that the f should be large for large M_{Z_H}, but if the s becomes small, for instance, less than 0.15 fb, f may also be small in a narrow parameter space. However, this influence on our results is not too large since we take a quite small s, for example, $s = 0.1$, in most of the calculations unless specifically stated.

(5) If we define $x = 4fv'/v^2$, where v' is the VEV of the scalar of the triplet ϕ, the masses of the neutral boson in the above equations can be rewritten by the parameter x and by this definition, the neutral scalar mass can be given as,

$$M^2_{\phi^0} = \frac{2m^2_{H^0} f^2}{v^2[1 - (4v'f/v^2)^2]} = \frac{2m^2_{H^0} f^2}{v^2(1 - x^2)}. \quad (11)$$

The above equation for the mass of ϕ^0 requires a constraint of $0 \leq x < 1$ (i.e., $4v'f/v^2 < 1$), which shows the relation between the scale f and the VEV of the Higgs field doublets and the triplet (v, v'), but this constraint is quite loose, in which the v' can be as large as 20–30 GeV for a small f value. The parameter $\rho \equiv m_z c_w/m_w$ (also the T parameter) dependence on the v', however, has been studied in Ref. [34], and we find that in a quite large space, the v' may lie in the range of several GeV, which constraints the parameter x cannot be too large. This is also the constraint coming from the T parameter, since T can be written as $\alpha T = \rho - 1 = \Delta\rho$. With the constraint of v' in the order of several GeV, here we can take x as a free parameter in the range $0 < x < 0.2$, which also indicates clearly that a larger x is not allowed by the current experiments.

(6) In the LH model, the relation among the Fermi coupling constant G_F, the gauge boson W mass

M_W, and the fine structure constant α can be written as [26,41]

$$\frac{G_F}{\sqrt{2}} = \frac{\pi\alpha}{2M_W^2 s_W^2}\left[1 - c^2(c^2 - s^2)\frac{v^2}{f^2} + 2c^4\frac{v^2}{f^2} - \frac{5}{4}(c'^2 - s'^2)\frac{v^2}{f^2}\right]. \quad (12)$$

So we have

$$\frac{e^2}{s_W^2} = \frac{4\sqrt{2}G_F M_W^2}{[1 - c^2(c^2 - s^2)\frac{v^2}{f^2} + 2c^4\frac{v^2}{f^2} - \frac{5}{4}(c'^2 - s'^2)\frac{v^2}{f^2}]}. \quad (13)$$

(7) Finally, the recent data of the 125 GeV Higgs also put some constraints on the parameter space [31], but the constraints are quite loose; for example, Figs. 1 and 2 in Ref. [31] give the dependence of the ratio R [$R = \mathrm{Br}(h \to \gamma\gamma(ZZ))_{\mathrm{LH}}/\mathrm{Br}(h \to \gamma\gamma(ZZ))_{\mathrm{SM}}$] on the f, and we find that they put quite loose constraints to the parameters, so we will not discuss this further.

C. Numerical results in the littlest Higgs model

Due to the interactions in Tables I and II, the single charged boson production associated with the W boson processes can proceed through various parton processes at the LHC, as shown in Fig. 2, in which those obtained by exchanging the two external gluon lines are not displayed. To know their relative values, here we first discuss the contributions from every single parton channel, though, actually, we cannot distinguish the initial states; i.e., we will first discuss the gg fusion and the $q\bar{q}$ annihilation processes, respectively, and then sum them all together to see the total contributions.

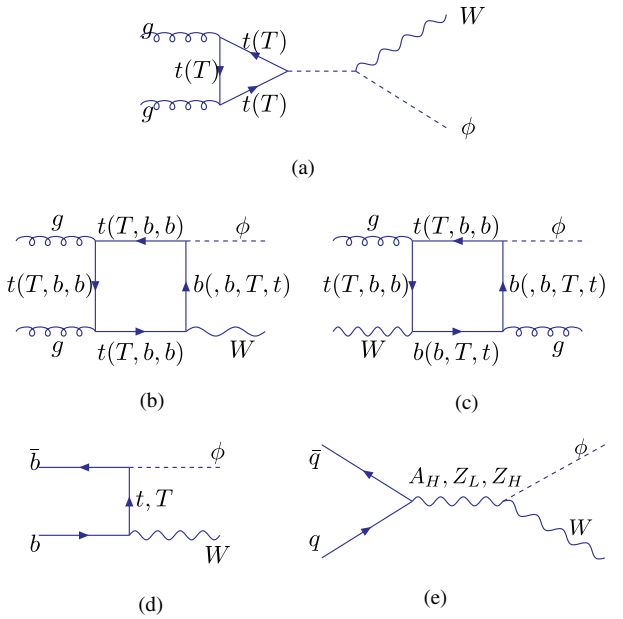

FIG. 2 (color online). Feynman diagrams for the charged scalar production associated with the W boson at the LHC via gluon fusion (a),(b),(c) and the quark antiquark annihilation (d),(e) parton level processes in the LH model. Those obtained by exchanging the two external gluon lines are not displayed here.

1. gg fusion in the LH models

Note that the processes consist of the box diagrams and the W scalar coupling, just shown as Figs. 2(a)–2(c). The s-channel contribution of the cross sections, however, is tiny, which is easy to understand with the quite large center-of-mass suppression.

The production cross sections of the ϕ^+W^- of the gg fusion are plotted in Fig. 3 for $E_{\mathrm{cm}} = 8$, 14 TeV, respectively, with $x = 0$, 0.05, 0.1, 0.2, and $f = 500$ GeV as functions of the scalar mass m_ϕ, assuming the charged and neutral scalar mass degenerate, $m_{\phi^\pm} = m_{\phi^0} = m_{\phi^p}$. From Fig. 3, we can see that the cross section of this process is quite large, about 100 fb in most of the parameter space and, as expected, the production rate decreases with the increasing scalar mass since the phase space is suppressed by the final masses.

To compare the other parameter dependence, in Figs. 3(c) and 3(d), we give the cross sections depending on the parameter f and s, for $E_{\mathrm{cm}} = 8$, 14 TeV, $f = 500$ GeV, and $m_\phi = 200$ GeV, which clearly shows the production rate varying as the different parameters. We can see the increasing production rate with the increasing s, but the cross section is decreasing when f grows up.

Figure 4 shows the parameter x dependence of the cross sections, forgetting the experimental constraints temporally, taking its value from 0 to 0.9 instead. From both Figs. 3 and 4 we can also see that the x dependence of the process $gg \to \phi^+W^-$ is strong, since the $x(= 4fv'/v^2)$ is closely connected to the triplet VEV v', and the v' decides the mixing parameter s_+, the parameter involved in the $\phi^+\bar{t}(T)b$. The production cross sections of the processes $gg \to W^+\phi^- + X$ decrease with the increasing parameter x. For example, when the center of mass is 8 TeV for $x = 0$, $m_\phi = 200$ GeV, and $s = 0.1$, the production rate is about 42 fb. When $x = 0.2$, however, the production rate declines to only 27 fb. The larger x is, the smaller the cross section is. The situation is the same even when x increases to 1, though the experiments constrain this parameter far below 1. When the center of mass is 14 TeV, the same situation occurs, and just the rate will be about an order larger than those of the smaller center of mass, i.e., 8 TeV.

As we have discussed, a too large x is excluded by the current data, so a vertical line is added in Fig. 4, and the allowed areas are on the left of the line, while they are disallowed on the right. The same situations occur in Figs. 6 and 8.

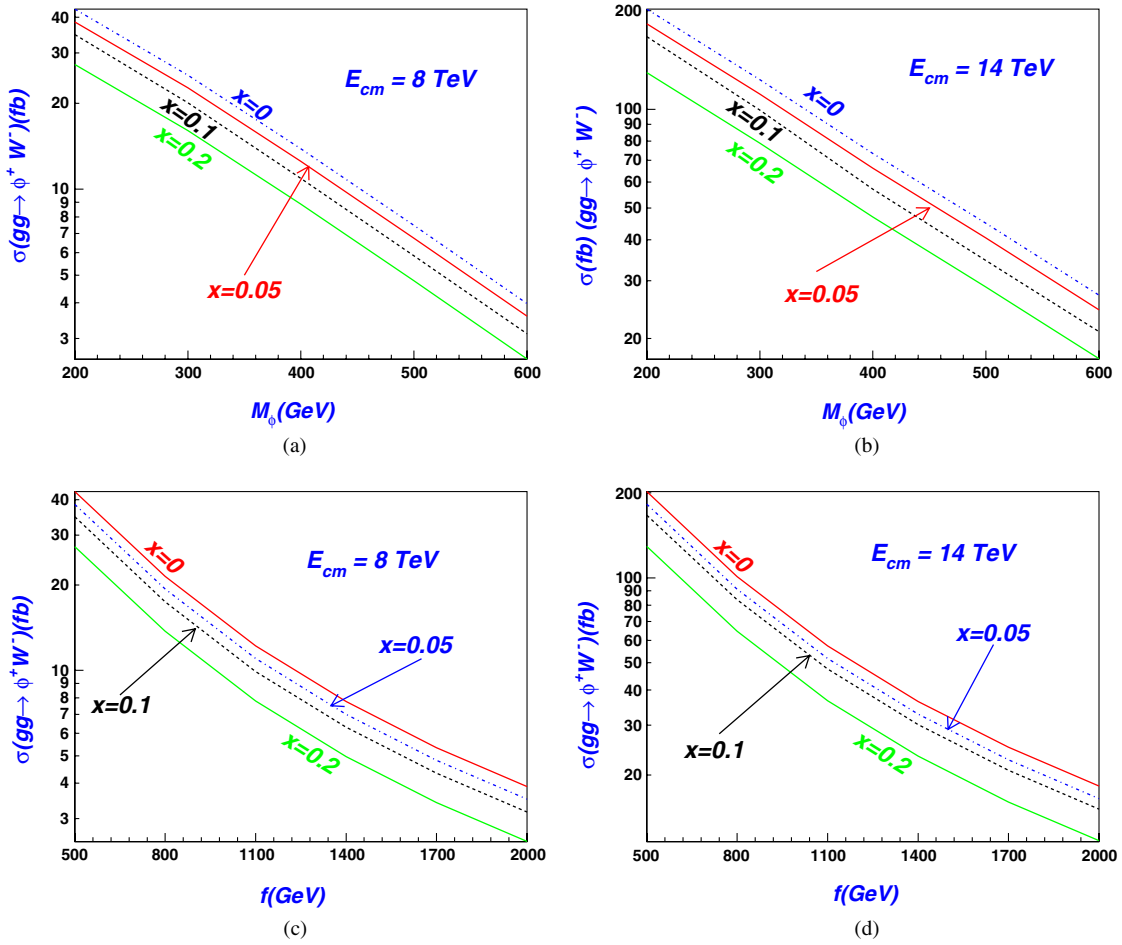

FIG. 3 (color online). In the LH, the cross section σ of the processes $gg \to \phi^+ W^-$ as a function of the scalar mass m_ϕ with the center-of-mass energy $E_{\rm cm} = 8$ TeV (a) and 14 TeV (b), respectively, for $f = 500$ GeV and $s = 0.1$, with different x ($x = 0$, 0.05, 0.1, 0.2); the cross section σ of the processes $gg \to \phi^+ W^-$ as a function of f with $E_{\rm cm} = 8$ TeV (c) and 14 TeV (d), respectively, and $s = 0.1$, with different x ($x = 0$, 0.05, 0.1, 0.2).

The mixing s affects the process $gg \to \phi^+ W^-$ largely, too; however, the trend is different. We can see from Fig. 4(c) that the possibility of the $\phi^+ W^-$ associated production increases with increasing s. In Figs. 3, 4(a), and 4(b), we take $s = 0.1$, which is quite small compared to its maximum value 0.5, according to the discussion of Refs. [34,35]. So our results are not the maximum case, they are general.

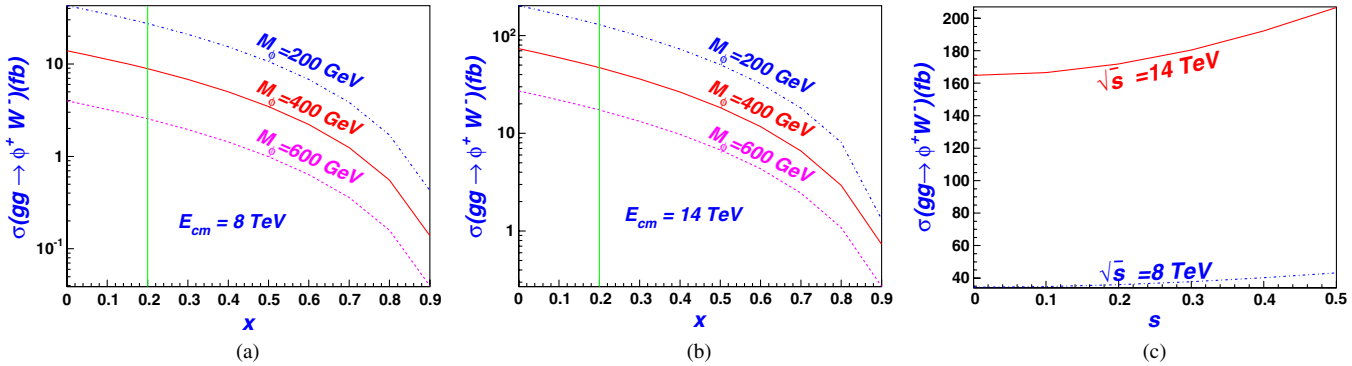

FIG. 4 (color online). In the LH, when the scalar mass $m_\phi = 200$, 400, 600 GeV, the cross section σ of the processes $gg \to \phi^+ W^-$ as a function of x with $E_{\rm cm} = 8$ TeV (a) and 14 TeV (b), respectively, and $s = 0.1$, with $f = 500$ GeV. The cross section σ of the processes $gg \to \phi^+ W^-$ as a function of s for $x = 0.1$, $f = 500$ GeV, and $E_{\rm cm} = 8$ and 14 TeV (c).

Similarly, we can see from Figs. 3(c) and 3(d) that the process $gg \to \phi^+ W^-$ is strongly dependent on the parameter f, which is understandable since most of the couplings in the LH models, such as $\phi^+ \bar{t}(T)b$ and $\phi^+ W^- S$ ($S = \phi^0$, ϕ^p, H), etc., are tightly connected with the parameter f. The cross sections may be large if the scale f is not too high and decrease as rapidly as the increasing f. The rates of the $\phi^+ W^-$ production for $\sqrt{s} =$ 14 TeV, for example, can arrive at about 273, 35, and 24 fb for $f = 500$, 1000, and 2000 GeV, respectively, with $s = 0.1$.

2. ϕW production via quark antiquark annihilation

In the LH, the ϕW production via quark antiquark annihilation is realized by the parton level $u\bar{u}$, $d\bar{d}$, $c\bar{c}$, $s\bar{s}$, $b\bar{b} \to \phi W$, which can be distinguished as t-channel and s-channel processes, but the t channel is only realized by the $b\bar{b}$ initial state, via $\phi^+ \bar{t}(T)b$ couplings.

Additionally, for the s-channel scalar and W boson associated production induced by the $q\bar{q}$ ($q = u$, d, s, c, b) collision, what makes the difference among them is only if we neglect the masses of the quarks u, d, c, s, b, the parton distribution function in the proton, so it is natural to see in Fig. 5 that $\sigma(u\bar{u}) > \sigma(d\bar{d}) > \sigma(s\bar{s}) > \sigma(c\bar{c}) > \sigma(b\bar{b})$.

In Figs. 5(a) and 5(b), we can see that the cross sections decrease with increasing charged scalar mass m_ϕ; the level of decline, however, is different. For $b\bar{b}$ realization, we can see it declines rapidly, while the $u\bar{u}$, $d\bar{d}$, $s\bar{s}$, $c\bar{c}$ annihilations are not so quick. It can be understood that with the small distribution in the proton, the $b\bar{b}$ collisions mainly contribute via the t channel, while the others are from s channels mediated by the bosons A_H, Z_L, Z_H, which appear in the propagator, with large masses of about 1 TeV, which weakens the effect of the increasing scalar mass. When m_ϕ is not too large compared to the heavy boson mass, the cross sections from the s-channel $q\bar{q}$ annihilations are almost unchanged. Actually, if we assume the ϕ^+ mass is of the order of the heavy bosons, i.e., more than 1 TeV, the situation is different immediately. With the increasing m_ϕ, the production rates decrease significantly, which is verified by our calculation, though not shown here.

The s-channel processes in Fig. 2(e) (though the parton distribution functions are larger for the $u\bar{u}$ and $d\bar{d}$ initial states) may be relatively small in view of the center-of-mass suppression effects. At the same time, the t-channel

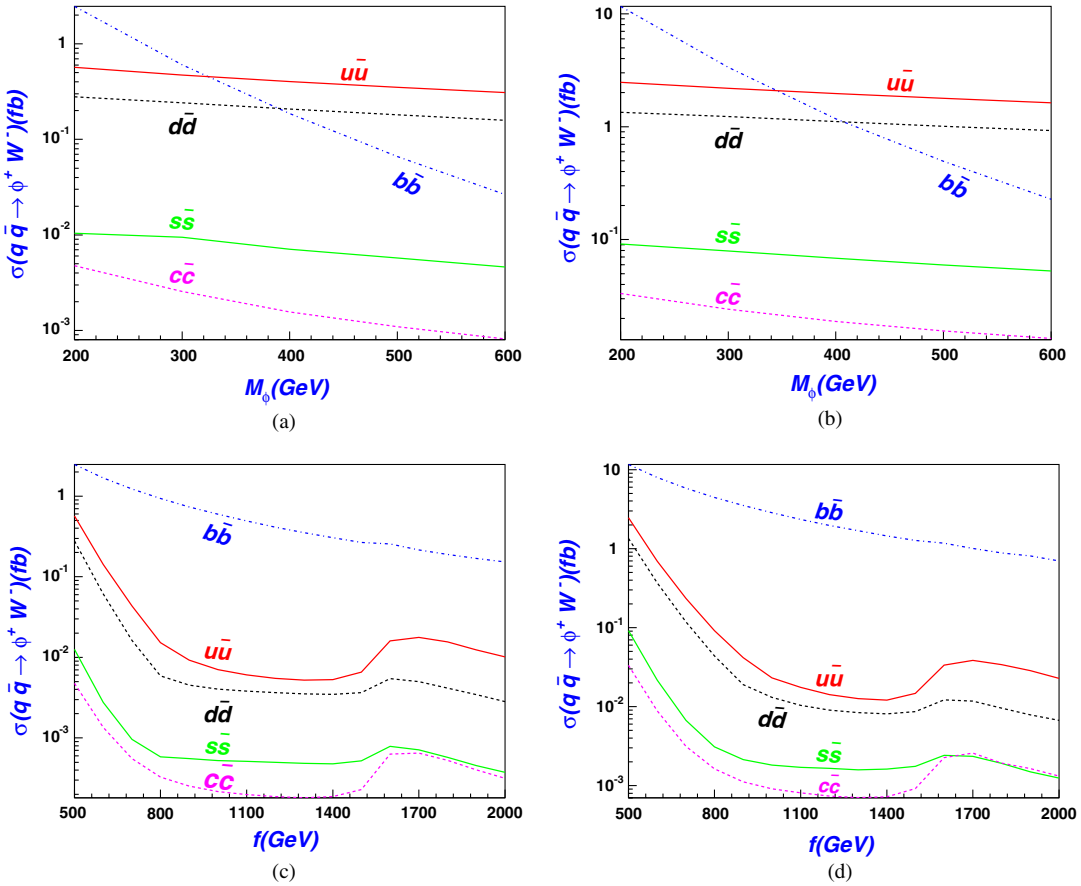

FIG. 5 (color online). In the LH, the cross section σ of the processes $q\bar{q} \to \phi^+ W^-$ as a function of the scalar mass m_ϕ with $E_{\rm cm} = 8$ TeV (a) and 14 TeV (b) for $f = 500$ GeV, $x = 0.1$, and $s = 0.1$. The $q\bar{q} \to \phi^+ W^-$ cross section σ as a function of f with $E_{\rm cm} = 8$ TeV (c) and 14 TeV (d), respectively, and $s = 0.1$, $x = 0.1$. Here $q = u$, d, c, s, b quarks.

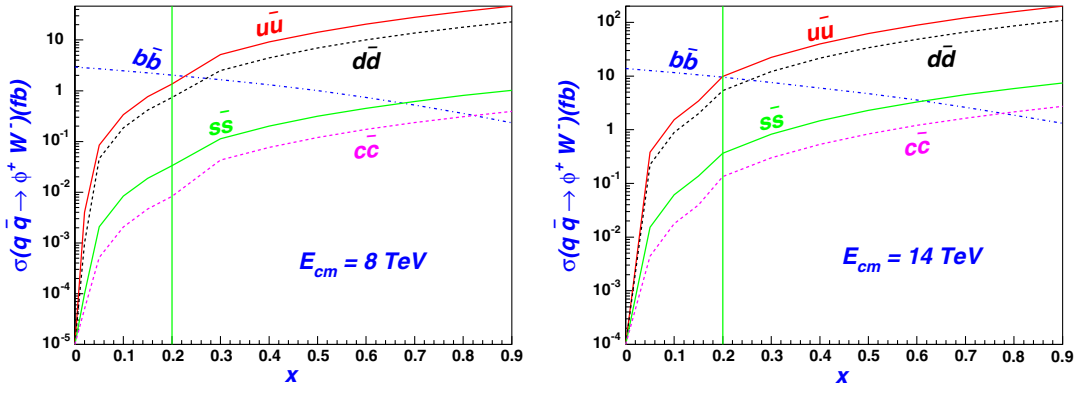

FIG. 6 (color online). In the LH, the cross section σ of the processes $q\bar{q} \to \phi^+ W^-$, with $m_\phi = 200$ GeV, $f = 500$ GeV as a function of x for $E_{\rm cm} = 8$ TeV (a) and 14 TeV (b) ($s = 0.1$).

coupling strengths may be large for little x. In Fig. 2(d), for instance, the strength of $\phi^+ \bar{t}(\bar{T})b \sim m_t/v \sim 1$ contributes significantly, so no wonder the cross sections of the parton level processes like $u\bar{u}(d\bar{d}, s\bar{s}) \to \phi W$ are smaller than those of the others even with larger parton distribution functions, especially with the increasing f. These can be seen clearly in Figs. 5(c) and 5(d).

Note that in Fig. 5 the processes depend largely on the parameter f, and if the parameter f decreases, the production rate of this process will go up rapidly. From the

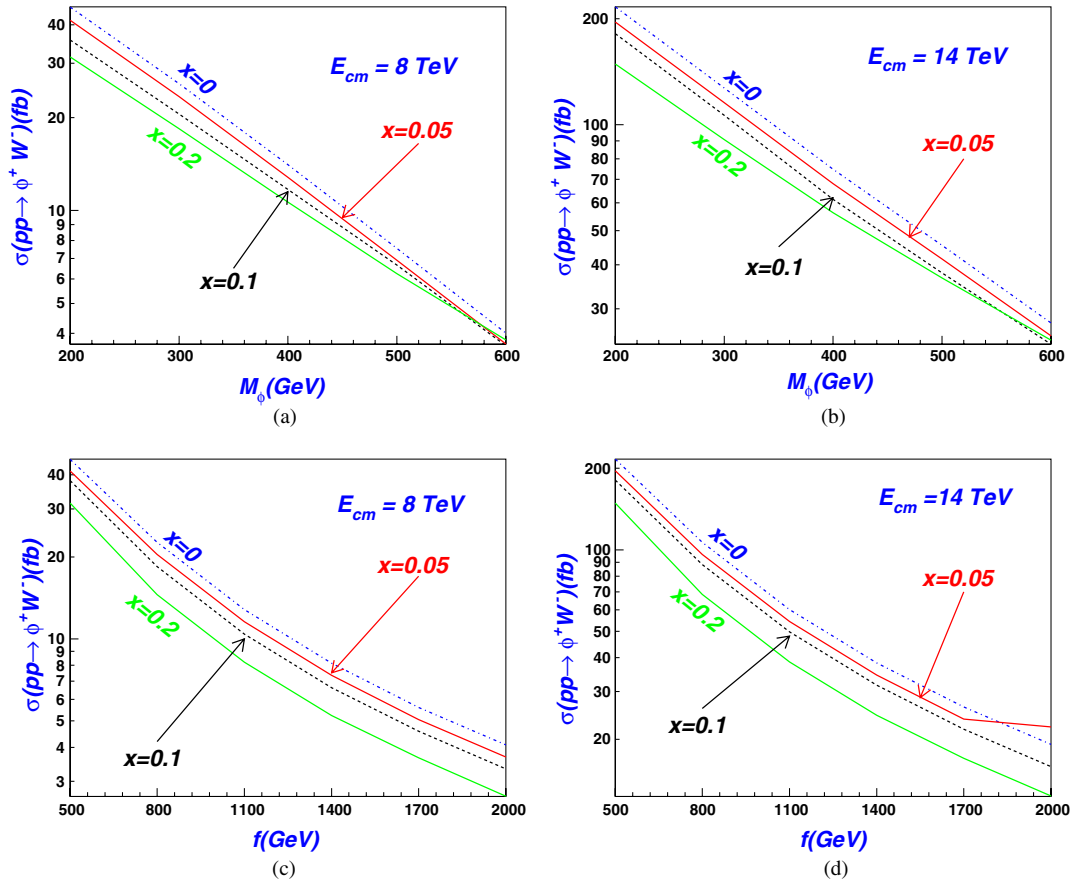

FIG. 7 (color online). In the LH models, the total cross section σ of the processes $pp \to \phi^+ W^-$ as a function of the scalar mass m_ϕ with $E_{\rm cm} = 8$ TeV (a) and 14 TeV (b) for $s = 0.1$, $f = 500$ GeV, and $x = 0$, 0.05, 0.1, 0.2. The total cross section σ of the processes $pp \to \phi^+ W^-$ as a function of f with the scalar mass $m_\phi = 200$ GeV, $s = 0.1$ and $E_{\rm cm} = 8$ TeV (c) and $E_{\rm cm} = 14$ TeV (d) for $x = 0, 0.05, 0.1, 0.2$.

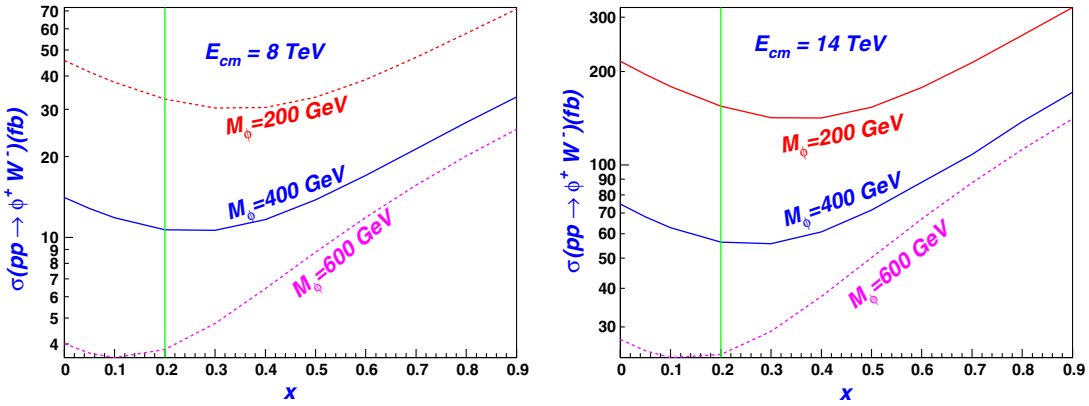

FIG. 8 (color online). The total cross section σ of the processes $pp \to \phi^+ W^-$ as a function of x with the scalar mass $m_\phi = 200$, 400, 600 GeV, $s = 0.1$, and $E_{\rm cm} = 8$ TeV (a) and $E_{\rm cm} = 14$ TeV (b).

couplings, it can also be seen clearly that the $\phi\bar{T}(\bar{t}) \sim 1/f$, while in the s channel, the couplings $V\phi W$ ($V = A_H$, Z_L, Z_H) $\sim v'$, $v' = xv^2/(4f)$, so they decrease with increasing f. The exception, however, occurs in Figs. 5(c) and 5(d), and therefore, Fig. 6.

From Fig. 5, we can also see that when x is small, such as 0.1, which we have chosen, in most of the parameter space, the largest channel of the processes $qq \to \phi W$ is the $b\bar{b} \to \phi W$, which is easy to understand since, in Fig. 2, the t-channel process 2(d) is free of the center-of-mass suppression and the upraise via x, i.e., the v', does not reveal itself. For larger x, however, the situation changes. We can see from Fig. 6 that, except via $b\bar{b}$ annihilation, the quark antiquark processes are increasing with the increasing x.

Figure 6 is the cross sections of the quark antiquark annihilations on the parameter x, taking x from 0 to 0.9, too. In Fig. 6, we can see that with the increasing parameter $x = 4fv'/v^2$, the trends of the cross sections are different from those in Fig. 4. When $x > 0.2$, the cross sections from the $u\bar{u}$ collision begin overwhelming that from $b\bar{b}$ at 14 TeV, which is opposite that of the above discussion. The reason is given as follows: it is the same as comparing ϕW production via gg fusion and $q\bar{q}$ annihilation.

Now, comparing Fig. 4(c) with Figs. 6 and 8, we find that the ϕW associated production from gg fusion and $b\bar{b}$ annihilation decreases with increasing x, while those from other quark antiquark annihilation ($u\bar{u}$, $d\bar{d}$, $s\bar{s}$, and $c\bar{c}$) are the opposite, which is understandable from their different coupling forms. Since the $VW_L\phi^+$ ($V = A_L$, Z_L, Z_H) is proportional to v', while $\phi\bar{t}(T)b$ is in proportion to $\frac{v}{f} - 2s_+$, here $s_+ = 2v'/v$. In the scalar-fermion couplings, actually, there is a competition between the two terms $\frac{v}{f}$ and $2s_+$. When $f = 500$ GeV, $v/f \sim 0.5$; the $2s_+$, however, is less than 0.5 all the time if we satisfy the requirement $v' < 30$, i.e., $x < 1$ [26], so with the increasing v', the coupling $\phi\bar{t}(T)b$ is decreasing.

3. Total contribution of the gg and quark antiquark annihilation

In Figs. 7 and 8, we sum the contributions from all the parton level processes. We can see from the figures that the cross sections can arrive at tens of fb even when $E_{\rm cm} =$ 8 TeV, and when the center of mass rises to 14 TeV, the production rates will become larger, larger than 100 fb in quite a large parameter space. So in the discussion of reducing the backgrounds, we will concentrate on the 14 TeV center of mass.

With the increasing x, the s-channel contributions of the $q\bar{q}$ annihilation become larger, so then the, so then the gg fusion and $b\bar{b}$ collision in the dominant t channel are not the largest anymore, but instead, the uu and dd will control the situation, which can be seen clearly in Fig. 7.

From Fig. 7 we can see that the production rates of the ϕ^+W^- decrease when m_ϕ or f goes up. Note that in Figs. 7(c) and 7(d), with the increasing f, in the tail of the curve for $pp \to \phi^+W^-$, $x = 0.7$, the cross sections increase when f changes from 1500 to 1700 GeV, which is understandable. When x is large, the contributions from the s channel surpass that from the t channel, i.e., the gg and $b\bar{b}$ realization.

III. THE LRTH MODEL AND ϕW PRODUCTION AT THE LHC

A. The LRTH model and the relevant couplings

To solve the little hierarchy problem [42], the left-right twin Higgs models was proposed [43,44]. In this model, the Higgses emerge again as pseudo Goldstone bosons and the leading order of the the Higgses' masses is quadratically divergent. One introduces an additional discrete symmetry so that the leading quadratically divergent terms respect the global symmetry. With the cancellation of the quadratically divergent terms, the Higgs masses possess logarithmically divergent contributions.

In such models, the global symmetry breaks from $U(4) \times U(4)$ to $U(3) \times U(3)$, and gauge symmetry from $SU(2)_L \times SU(2)_R \times U(1)_{B-L}$ to $SU(2)_L \times U(1)_Y$. Fourteen Goldstone bosons are generated, three of which are eaten by the massive gauge bosons Z_H and $W_H^{\pm}$, while the rest of the Goldstone bosons contain the SM $SU(2)_L$ Higgs doublet and extra Higgses.

To cancel the leading quadratic divergence of the SM gauge bosons and the top quark contributions to the Higgs masses in the loop level, the new heavy gauge bosons and a vector top singlet pair are introduced. Thus, the hierarchy problem is solved. The new particles in the LRTH model (the gauge bosons and the vector top singlet) have rich phenomenology at the LHC and people are interested in them.

The two Higgs fields H and $\hat{H}$ acquire two nonzero VEVs which break the $U(4) \times U(4)$ to $U(3) \times U(3)$ and yield 14 Goldstone bosons, six of which are eaten by the massive gauge bosons. Finally, there is one neutral pseudoscalar ϕ^0, a pair of charged scalar $\phi^{\pm}$, and the SM physical Higgs h, whose representation of (ϕ^+, ϕ^0) is $(1, 2, 1)$ in the gauge group $SU(3)_L \times SU(3)_R \times U(1)_{B-L}$. An $SU(2)_L$ doublet $\hat{h} = (\hat{h}_1^+, \hat{h}_2^0)$ is also left in the Higgs spectrum.

The quantum numbers of the gauge bosons of $W^{\pm}$ and $W_H^{\pm}$ are $(3, 1, 0)$ and $(1, 3, 0)$. After the symmetry breaking, the six physically massive gauge bosons are four charged and two neutral ones: $W^{\pm}$, $W_H^{\pm}$, Z, and Z_H. W and Z are the usual massive gauge bosons in the SM, and W_H and Z_H are three additional new massive gauge bosons with masses of TeV.

The Lagrangian of the new particles can be written as

$$\mathcal{L} = \mathcal{L}_H + \mathcal{L}_G + \mathcal{L}_f + \mathcal{L}_Y + \mathcal{L}_{\text{one-loop}} + \mathcal{L}_{\mu}. \quad (14)$$

The various terms in Eq. (14) are covariant kinetic terms for Higgses, gauge bosons and fermions, Yukawa interactions, one-loop Coleman-Weinberg potential [44,45] for Higgses, and soft symmetry breaking μ terms. The explicit expression can be found in Ref. [44] and here we do not list it.

Based on the Lagrangian given in Ref. [44], we have the couplings with the fermions involved in our calculation in Table III.

TABLE III. The three-point couplings of the charged gauge boson-fermion-fermion and those of the scalar-fermion-fermion in the LRTH models. The chirality projection operators are $P_{R,L} = (1 \pm \gamma_5)/2$.

Particles	Vertices	Particles	Vertices
$W_{+\mu}\bar{t}b$	$e\gamma_\mu C_L P_L/(\sqrt{2}s_w)$	$W^{+\mu}\bar{T}b$	$e\gamma_\mu S_L P_L/(\sqrt{2}s_w)$
$H\bar{t}t$	$-em_t C_L C_R/(2m_W s_w)$	$H\bar{T}T$	$-y(S_R S_L - C_L C_R x)/\sqrt{2}$
$\Phi^0\bar{t}t$	$-iyS_R S_L \gamma_5/\sqrt{2}$	$\Phi^0\bar{T}T$	$-iyC_L C_R \gamma_5/\sqrt{2}$
$\Phi^+\bar{t}b$	$-i(S_R m_b P_L - yS_L f P_R)/f$	$\Phi^+\bar{T}b$	$i(C_R m_b P_L - yC_L f P_R)/f$

As for the coupling between the boson and the scalars, we find that they all vanish if we parametrize the scalars in the Goldstone bosons fields as [44]

$$\begin{aligned} N &\to \frac{\sqrt{2}\hat{f}}{F(\cos x + 2\frac{\sin x}{x})}\phi^0, \quad \hat{N} \to -\frac{\sqrt{2}f\cos x}{3F}\phi^0, \\ h_1 &\to 0, \quad h_2 \to \frac{v+h}{\sqrt{2}} - i\frac{x\hat{f}}{\sqrt{2}F(\cos x + 2\frac{\sin x}{x})}\phi^0, \\ C &\to -\frac{x\hat{f}}{F\sin x}\phi^+, \quad \hat{C} \to \frac{f\cos x}{F}\phi^+, \end{aligned} \quad (15)$$

where the N, $\hat{N}$, h_1, h_2, C, $\hat{C}$ are in the Goldstone bosons fields,

$$\begin{aligned} H &= i\frac{\sin\sqrt{\chi}}{\sqrt{\chi}}e^{i\frac{N}{2f}}\begin{pmatrix} h_1 \\ h_2 \\ C \\ N - if\sqrt{\chi}\cot\sqrt{\chi} \end{pmatrix}, \\ \hat{H} &= i\frac{\sin\sqrt{\hat{\chi}}}{\sqrt{\hat{\chi}}}e^{i\frac{\hat{N}}{2f}}\begin{pmatrix} \hat{h}_1 \\ \hat{h}_2 \\ \hat{C} \\ \hat{N} - i\hat{f}\sqrt{\hat{\chi}}\cot\sqrt{\hat{\chi}} \end{pmatrix}. \end{aligned} \quad (16)$$

By this parametrization, the requirement of vanishing gauge-Higgs mixing terms can be satisfied; i.e., in this redefinition of the Higgs fields, the couplings $WZ\phi^+$, $W\gamma\phi^+$, $WZ_H\phi^+$, $W\gamma_H\phi^+$, $W\phi^0\phi^+$, and $Wh\phi^+$ are zero, which has been verified by our written calculation. This is quite different from that in the littlest Higgs models.

B. LRTH ϕW production at the LHC and the numerical results

Due to the missing gauge-Higgs mixing terms, the associated production of the charged scalar ϕ^+ and the charged gauge boson W is different from that in the little Higgs models. Figures 2(a) and 2(e) will not occur in the LRTH models since they contain the gauge-Higgs mixing couplings, while the others are kept and they are the realization of the ϕW production in the LRTH models.

When discussing the numerical results of the processes, just as the discussions of the LH models, we also first investigate the contributions from every single parton channel, i.e., the gg fusion and the $q\bar{q}$ annihilation processes, respectively, and then sum them for the total contributions.

1. gg fusion in the LRTH models

Different from that of the LH models, the ϕW associated production is carried out only by the box diagrams from gg fusion and t-channel contribution via the quark antiquark annihilation, just as shown in Figs. 2(b)–2(d), and the s channels in Figs. 2(a) and 2(e) are missing.

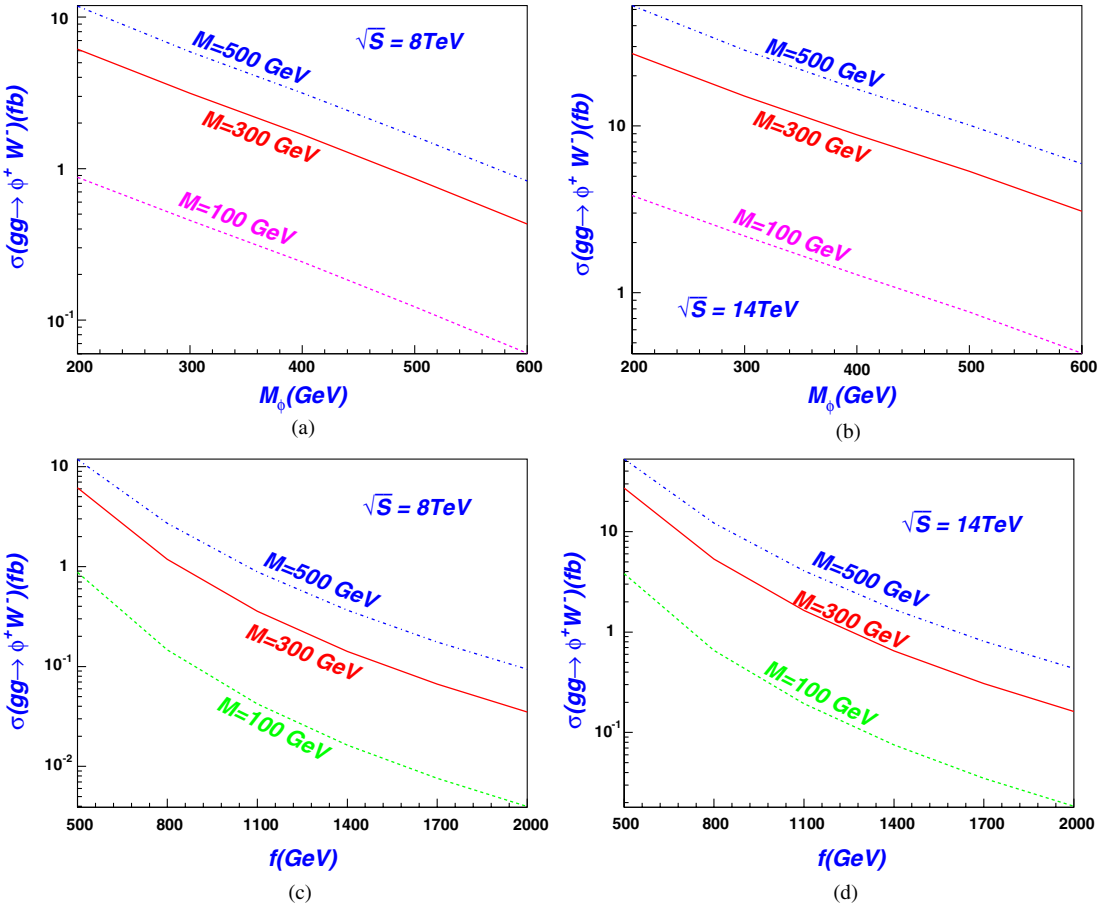

FIG. 9 (color online). In the LRTH, the cross section σ of the processes $gg \to \phi^+ W^-$ as a function of the scalar mass m_ϕ (a),(b) or f (c),(d) with $E_{\rm cm} = 8$ TeV and $E_{\rm cm} = 14$ TeV for $M = 100$, 300, 500 GeV.

The production cross sections of the $\phi^+ W^-$ of the gg fusion are plotted in Fig. 9 with $M = 100$, 300, 500 GeV for $E_{\rm cm} = 8$, 14 TeV and for $f = 500$ GeV, as functions of the scalar mass m_ϕ, assuming the charged and neutral scalar mass degenerate, $m_{\phi^\pm} = m_{\phi^0} = m_{\phi^p}$. From Fig. 9, we can see the cross section of this process is less than 50 fb in most of the parameter space, even for a larger center-of-mass energy, i.e., at 14 TeV with $M = 500$ GeV. We can also see that, as expected, the production rate decreases with the increasing scalar mass since the phase space is suppressed by the mass.

Figure 9 shows the different dependence of the cross sections on the parameter M, with $M = 100$, 300, 500 GeV. The results change with the varying values of M and when M is large, such as the cross section can arrive at 53 fb, while when M=100 GeV, the production can be less than one tenth of the former, with other parameters being the same.

When M is very small, such as $\lesssim 1$ GeV, the collider phenomenology of the $\phi^+ W^-$ will be very small, which can be seen clearly via the two group couplings that realize the $\phi^+ W^-$ associated production. The $\phi^+ \bar{t} b$ and $W^-_\mu t \bar{b}$ couplings, for example, are $(S_R m_b P_L - y S_L f P_R)/f$ and $\gamma_\mu C_L P_L/(\sqrt{2} s_w)$, respectively, with S_L, $S_R \sim M/M_T$ and $C_L = \sqrt{1 - S_L^2}$. So when M is small, S_L, S_R will become small too. When $M = 0$, S_L, S_R also change into zero. So if M is too small, the signal will be very small. In the limit case, when $M = 0$, the light top will not mix with the heavy top, so the couplings $\phi^+ \bar{t} b$ disappear, and the contribution is only from the heavy top coupling to the scalar. While the light charged boson,which mainly couples to the light top, the heavy top and light boson couplings $W^+ \bar{T} b$ proportional to $S_L \sim M$ disappear when M=0. Therefore, the cross section will drop down to zero when M is in its limit $M = 0$.

We can also see from Fig. 9 that the process $gg \to \phi^+ W^-$ is strongly dependent on the parameter f, which is understandable, since most of the couplings in the LRTH models, such as $\phi^+ t \bar{b}$, $\phi^+ T \bar{b}$, etc., are tightly connected with the parameter f. The cross sections may be larger unless f is not high enough. The rates of the $\phi^+ W^-$ production for $\sqrt{s} = 14$ TeV and $m_\phi = 200$ GeV, for example, are 52 and 7 fb, for $f = 500$ GeV and $f = 1000$ GeV, respectively.

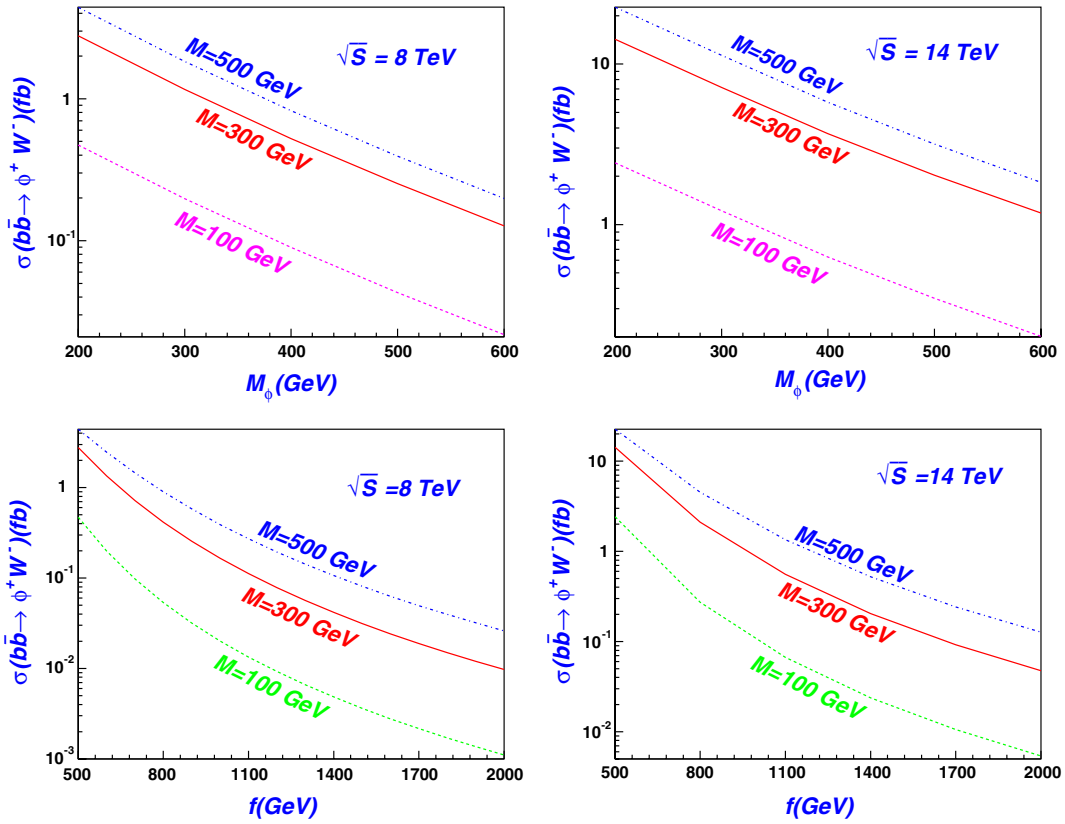

FIG. 10 (color online). In the LRTH, the cross section σ of the processes $q\bar{q} \to \phi^+ W^-$ as a function of m_ϕ or f for $M = 100$, 300, 500 GeV with the scalar mass $m_\phi = 200$ GeV and $E_{\rm cm} = 8$ TeV and $E_{\rm cm} = 14$ TeV.

2. $b\bar{b}$ annihilation in the LRTH models

Unlike that in the LH models, in the LRTH, the ϕW production via quark antiquark annihilation is realized only by the t-channel parton level $b\bar{b} \to \phi W$, which is because we have expected the gauge-Higgs coupling to vanish, so the s-channel processes are missing, and only the t-channel processes proceeded by the t-b and T-b mixings survive.

Due to the small parton distribution functions, the $b\bar{b}$ realization of the ϕW production, which is at tree level, is not large enough and can arrive at about 20 fb, which is a little smaller than that of the gg fusion in the loop-level realization.

At the same time, we can see that the process $b\bar{b} \to \phi W$ depends largely on the parameters M and f, and if f goes up, the production rate of this process will decrease, but for parameter M, the cross sections will increase with the increasing parameter M, which can be also seen in Fig. 10.

3. Total contribution of the gg and quark antiquark annihilation

In LRTH models, we sum all of the contributions from gg fusion and $b\bar{b}$ annihilation for the $\phi^+ W^-$ associated production in Fig. 11, and from which we can see that the cross section arrives at tens of fb, dependent on the parameters f, M and the scalar mass in a certain center-of-mass $E_{\rm cm}$. But in quite a large parameter space, the cross sections are less than 10 fb. Normally, at the LHC, this would not interest us, so we will only discuss it briefly in the following section.

IV. BACKGROUNDS AND DETECTIONS

From the data above, we can see that at $E_{\rm cm} = 8$ TeV, no matter which model, LH or LRTH, the cross section of the charged Higgs associated with a W boson production is quite small, even with a little scalar mass, such as 200 GeV, supposing the luminosity is 10 fb^{-1}. It is easier, however, for the charged Higgs boson to be observed at $E_{\rm cm} =$ 14 TeV. Therefore, from now on we focus on investigating the charged Higgs associated with a W boson in the following processes at 14 TeV. The following signatures can be considered [46]:

$$\begin{aligned} pp &\to W^- H^+ \to W^- t\bar{b} \to l^- \nu b\bar{b}jj, \\ pp &\to W^+ H^- \to W^+ \bar{t}b \to l^+ \nu b\bar{b}jj, \end{aligned} \tag{17}$$

at $E_{\rm cm} = 14$ TeV with $200 \le m_\phi \le 600$ GeV.

For the processes above with final state $l + \not{E}_T + b\bar{b}jj$, the dominant SM backgrounds are $t\bar{t}$, $t\bar{t}W$, $t\bar{t}Z$, $WZjj$, $WWjj$, and $Wjjjj$, which are discussed in Ref. [46]. In

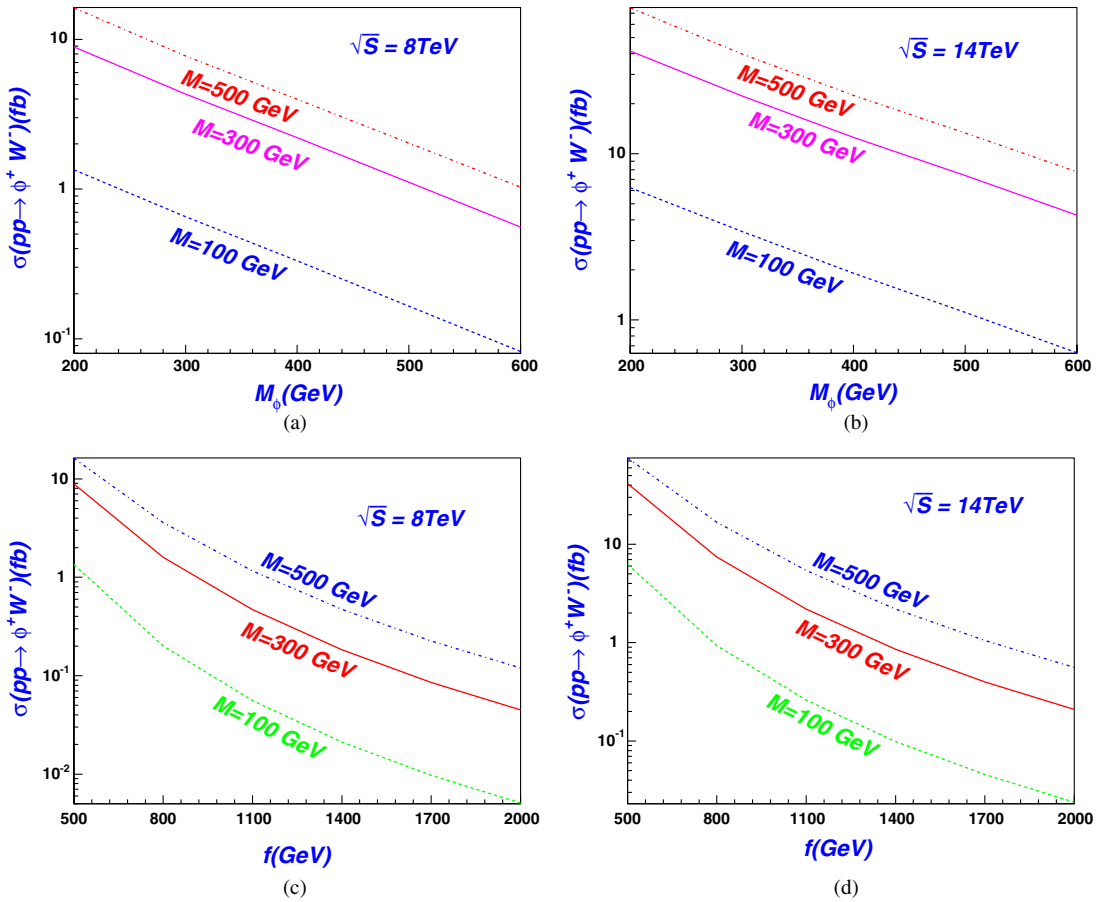

FIG. 11 (color online). In the LRTH, the total cross section σ of the processes ϕ^+W^- associated production from gg fusion and $b\bar{b}$ collision as a function of the scalar mass m_ϕ (a),(b) or f (c),(d) with $E_{\rm cm} = 8$ TeV and $E_{\rm cm} = 14$ TeV for $f = 500$, 1000 GeV for different M ($M = 100$, 300, 500 GeV).

the signature of the $H^\pm W^\mp$ production processes, the charged Higgs decays to four jets and the top quark decays to three jets. Thus, to make the signal clear, one can make the following requirements: (1) the invariant mass of the final four jets must be around the charged Higgs mass, and (2) three of the four jets must reconstruct into a top quark mass. To suppress the $t\bar{t}$ final state, the dominant channels of the backgrounds, one can construct the second top quark. The final results given in Ref. [46] show that after all cuts, the left cross section of the signal is 1 fb when $m_{H^\pm} = 500$ GeV, and the backgrounds are becoming negligibly small. Reference [46] also points out in Tables I and II, that with the increasing charged scalar mass, the backgrounds become smaller and easier to be suppressed, so it seems that the larger the charged scalar mass is, the easier it is to detect the $W\phi$ production at the LHC, though the cross section of the signals will also be smaller.

From Ref. [46] Table II, we can see that if the scalar mass is 400 GeV, the $S/\sqrt{B}$ can reach 3.42, and with the increasing m_S (scalar mass), the $S/\sqrt{B}$ gets larger, so we will focus on the scalar mass at 400 GeV and larger. From Table I of Ref. [46], we can see that if $m_S = 400$ GeV, when the cross section arrives at 49.7 fb, the $S/\sqrt{B}$ will be larger than 3.

Table IV gives the optimum value of the ϕ^+W^- production in the LH and LRTH models at 14 TeV when $m_\phi = 400$ GeV. The parameters are set as $s = 0.1$, $s' = 0.5$, $f = 500$, 1000 GeV in the LH models, and in the LRTH models, the involved parameters are $Y = 1$, $f = 500$, and 1000 GeV.

From Table IV, we can see that in the LH model, when $m_S = 400$ GeV, for the small scale f, the cross sections are

TABLE IV. For $m_\phi = 400$ GeV, the cross section of the signal process at $E_{\rm cm} = 14$ TeV for f and M in units of GeV, cross sections in units of fb.

LH	$x = 0$	$x = 0.05$	$x = 0.1$	$x = 0.15$	$x = 0.2$
$f = 500$	87.22	79.23	72.33	66.44	61.59
$f = 1000$	27.84	25.12	22.55	20.11	17.83
LRTH	$M = 0$	$M = 100$	$M = 300$	$M = 500$	$M = 700$
$f = 500$	0	1.9	12.5	22.4	29
$f = 1000$	0	0.10	0.86	2.07	3.36

larger than 49.7 fb, which is the value for the 3σ confidence level. While for the LRTH, it is dangerous to reach the detectable level in the largest parameter space. In LH models, when f is large, the production rates will be suppressed and smaller than 49.7 fb, which will be hard to probe. The cross sections, however, are also sensitive to the parameters s and s', and this would give quite larger results if we fine-tune the parameters. When $s = s' = 0.1$, for example, the production can even arrive at 1000 fb. However, this fine-tuning is not what we want, since it is only in a small parameter space and we should consider the confinements, such as those in Refs. [34,35].

In the LH models, however, we can also consider the larger scalar mass, such as 600 GeV, according to Tables I and II in Ref. [46]; the cross sections before the cuts are about 14 fb, and the $S/\sqrt{B}$ is 8.77 with the integral luminosity 300 fb^{-1}. We calculate the rate of the ϕW production at $m_\phi = 600$ GeV for $f = 1000$ GeV and $s = 0.1$. We just find that the cross section can arrive at about 9 fb, which is close to 14 fb, so we can imagine that the signal and backgrounds $S/\sqrt{B}$ should be large, at least larger than 3 for such a large cross section for $m_\phi = 600$ GeV. Therefore, we may conclude that for a larger scalar mass, the associated production could be more easily detected.

As for the other production modes of the charged Higgs in the LH and LRTH models, the pair production should be the most interesting one since the order may be large. For the two models, the large SM backgrounds do not require too much luck to detect, as stated in Ref. [24]; it may only be possible for the charged Higgs to be produced in quite a narrow space. The pair productions of the neutral Higgs are also discussed [24] and they are also possible in a narrow parameter space. Other production modes of the Higgs in the LH and LRTH models, such as ZH, tH, and ZHH [24], are also studied.

If one wants to detect all these procedures listed above, the common requirement is that both the f and the Higgs masses must not be too large, which is in agreement with the principle of W and the charged Higgs associated production, which has been discussed in this work. A larger f, e.g., $f > 1000$ GeV, however, is preferred by current constraints, so it may be another interesting issue to consider a larger boson mass to carry out the detection of this signal. As we have discussed, it may also be possible to probe the signal in small parameter spaces. Though f is relatively large ($f > 800$ GeV), in this work we show the results with a smaller f (f from 500 to 2000 GeV), too, to see the impact of this parameter on the associated production.

V. CONCLUSION AND SUMMARY

We calculate the charged scalar production associated with a gauge boson W in the LH models and the LRTH realizations. Comparing the two kinds of models, we can see that at the LHC, the ϕW production in the LH models are larger than that in the LRTH models, and it should be more possible to detect the LH models at the LHC via the $\phi^+ W^-$ production. From the discussion above, we can also conclude that in the LH models, for a small f, in most parameter space of the LH model, the production rates can arrive at the detectable level. But when f is large, the suppression effect becomes strong, so it may be difficult for the LHC to detect the signal. With a larger scalar mass, however, the signal will be a little easier to detect.

ACKNOWLEDGMENTS

This work was supported by the National Natural Science Foundation of China under the Grants No. 11105125, No. 11105124, and No. 11205023.

[1] G. Aad *et al.* (ATLAS Collaboration), Phys. Lett. B **716**, 1 (2012).
[2] S. Chatrchyan *et al.* (CMS Collaboration), Phys. Lett. B **716**, 30 (2012).
[3] N. Arkani-Hamed, A. G. Cohen, T. Gregoire, E. Katz, A. E. Nelson, and J. G. Wacker, J. High Energy Phys. 08 (2002) 021; J. G. Wacker, arXiv:hep-ph/0208235; M. Schmaltz, Nucl. Phys. B, Proc. Suppl. **117**, 40 (2003); M. Schmaltz and D. Tucker-Smith, Annu. Rev. Nucl. Part. Sci. **55**, 229 (2005).
[4] Z. Chacko, H.-S. Goh, and R. Harnik, Phys. Rev. Lett. **96**, 231802 (2006); Z. Chacko, Y. Nomura, M. Papucci, and G. Perez, J. High Energy Phys. 01 (2006) 126; Z. Chacko, H. Goh, and R. Harnik, J. High Energy Phys. 01 (2006) 108.
[5] C. Quigg, Contemp. Phys. **48**, 1 (2007); S. Matsumoto, M. M. Nojiri, and D. Nomura, Phys. Rev. D **75**, 055006 (2007).
[6] M. Acciarri *et al.* (L3 Collaboration), Phys. Lett. B **496**, 34 (2000); R. Barate *et al.* (ALEPH Collaboration), Phys. Lett. B **487**, 253 (2000).
[7] J. Abdallah *et al.* (LEP Higgs Working Group), arXiv:hep-ex/0107031.
[8] A. Abulencia *et al.* (CDF Collaboration), Phys. Rev. Lett. **96**, 042003 (2006); V. M. Abazov *et al.* (D0 Collaboration), Phys. Lett. B **682**, 278 (2009); T. Aaltonen *et al.* (CDF Collaboration), Phys. Rev. Lett. **103**, 101803 (2009); V. M. Abazov *et al.* (D0 Collaboration), Phys. Rev. D **80**, 051107 (2009).

[9] ATLAS Collaboration, Report No. CERN-LHCC-94-38 (1994); CMS Collaboration, Report No. CERN-LHCC-94-43 (1994).

[10] T. Plehn, Phys. Rev. D **67**, 014018 (2003).

[11] E. L. Berger, T. Han, J. Jiang, and T. Plehn, Phys. Rev. D **71**, 115012 (2005).

[12] G. P. Salam, Eur. Phys. J. C **67**, 637 (2010).

[13] C. K. Vermilion, arXiv:1101.1335.

[14] A. Abdesselam, E. B. Kuutmann, U. Bitenc, G. Brooijmans, J. Butterworth, P. B. de Renstrom, D. Buarque Franzosi, R. Buckingham *et al.*, Eur. Phys. J. C **71**, 1661 (2011).

[15] L. G. Almeida, R. Alon, and M. Spannowsky, Eur. Phys. J. C **72**, 2113 (2012).

[16] S. Yang and Q.-S. Yan, J. High Energy Phys. 02 (2012) 074.

[17] K. Jakobs, Eur. Phys. J. C **59**, 463 (2009); D. de Florian and M. Grazzini, Phys. Lett. B **674**, 291 (2009).

[18] A. Cagil and M. T. Zeyrek, Acta Phys. Pol. B **42**, 45 (2011).

[19] D. Lopez-Val and J. Sola, Proc. Sci., RADCOR2009 (2010) 045.

[20] A. Arhrib, R. Benbrik, C.-H. Chen, and R. Santos, Phys. Rev. D **80**, 015010 (2009).

[21] R. Guedes, S. Moretti, and R. Santos, J. High Energy Phys. 10 (2012) 119.

[22] G.-L. Liu, H.-J. Zhang, and P. Zhou, J. High Energy Phys. 07 (2012) 081.

[23] J. Huang, T. Song, S. Wang, and G. Lu, Chin. Phys. C **35**, 717 (2011).

[24] See, e.g., S.-M. Du, L. Guo, W. Liu, W.-G. Ma, and R.-Y. Zhang, Phys. Rev. D **86**, 054027 (2012); A. Cagil and H. Dag, arXiv:1203.2232; A. Cagil, Nucl. Phys. **B843**, 46 (2011); S. Yang, Phys. Lett. B **675**, 352 (2009); Q.-G. Zeng, C.-X. Yue, and J. Zhang, Nucl. Phys. **B860**, 152 (2012); L. Wang, L. Wu, and J. M. Yang, Phys. Rev. D **85**, 075017 (2012); Y.-B. Liu and X.-L. Wang, Nucl. Phys. **B839**, 294 (2010); H.-J. He and C.-P. Yuan, Phys. Rev. Lett. **83**, 28 (1999); J. L. Diaz-Cruz, H.-J. He, and C.-P. Yuan, Phys. Lett. B **530**, 179 (2002); C. Balazs, H.-J. He, and C.-P. Yuan, Phys. Rev. D **60**, 114001 (1999); A. A. Barrientos Bendezu and B. A. Kniehl, Phys. Rev. D **63**, 015009 (2000); **61**, 097701 (2000); R. Enberg, R. Pasechnik, and O. Stal, Phys. Rev. D **85**, 075016 (2012); Y. Liu, H. Han, and X. Wang, Eur. Phys. J. C **53**, 615 (2008).

[25] See M. Hashemi, Phys. Rev. D **83**, 055004 (2011); D. Eriksson, S. Hesselbach, and J. Rathsman, arXiv:0710.3346; J. Gao, C. S. Li, and Z. Li, Phys. Rev. D **77**, 014032 (2008); D. Eriksson, S. Hesselbach, and J. Rathsman, Eur. Phys. J. C **53**, 267 (2008); C. Yue, S. Wang, and D. Yu, Phys. Rev. D **68**, 115004 (2003).

[26] N. Arkani-Hamed, A. G. Cohen, E. Katz, and A. E. Nelson, J. High Energy Phys. 07 (2002) 034; S. Chang, J. High Energy Phys. 12 (2003) 057; T. Han, H. E. Logan, B. McElrath, and L. Wang, Phys. Rev. D **67**, 095004 (2003).

[27] J. Pumplin, D. R. Stump, J. Huston, H.-L. Lai, P. Nadolsky, and W.-K. Tung, J. High Energy Phys. 07 (2002) 012.

[28] T. Hahn and M. Perez-Victoria, Comput. Phys. Commun. **118**, 153 (1999).

[29] T. Aaltonen (CDF Collaboration), Phys. Rev. Lett. **105**, 252001 (2010).

[30] K Nakamura (Particle Data Group), J. Phys. G **37**, 075021 (2010).

[31] X.-F. Han, L. Wang, J. M. Yang, and J. Zhu, Phys. Rev. D **87**, 055004 (2013).

[32] J. Reuter and M. Tonini, J. High Energy Phys. 01 (2013) 077.

[33] A. Melfo, M. Nemevsek, F. Nesti, G. Senjanovic, and Y. Zhang, Phys. Rev. D **85**, 055018 (2012).

[34] T. Gregoire, D. R. Smith, and J. G. Wacker, Phys. Rev. D **69**, 115008 (2004); M. Chen and S. Dawson, Phys. Rev. D **70**, 015003 (2004); S. C. Park and J. Song, Phys. Rev. D **69**, 115010 (2004).

[35] C. Csaki, J. Hubisz, G. D. Kribs, P. Meade, and J. Terning, Phys. Rev. D **68**, 035009 (2003).

[36] A. Cagil and H. Dag, arXiv:1203.2232.

[37] N. Hod (ATLAS Collaboration), Eur. Phys. J. Web Conf. **49**, 15004 (2013).

[38] G. Aad (ATLAS Collaboration), J. High Energy Phys. 01 (2013) 029.

[39] S. Chatrchyan (CMS Collaboration), Report No. CMS-EXO-12-016 (2012); CMS Collaboration, Report No. CERN-PH-EP-2013-015 (2013).

[40] K. Yi (CMS Collaboration), J. Phys. Conf. Ser. **455**, 012034 (2013).

[41] R. Casalbuoni, A. Deandrea, and M. Oertel, J. High Energy Phys. 02 (2004) 032; C.-X. Yue and W. Wang, Nucl. Phys. **B683**, 48 (2004); W. Kilian and J. Reuter, Phys. Rev. D **70**, 015004 (2004); A. Deandrea, arXiv:hep-ph/0405120.

[42] See, e.g., H.-C. Cheng and I. Low, J. High Energy Phys. 09 (2003) 051.

[43] Z. Chacko, H. S. Goh, and R. Harnik, J. High Energy Phys. 01 (2006) 108; H.-S. Goh and C. A. Krenke, Phys. Rev. D **76**, 115018 (2007).

[44] H.-S. Goh and S. Su, Phys. Rev. D **75**, 075010 (2007).

[45] S. R. Coleman and E. Weinberg, Phys. Rev. D **7**, 1888 (1973).

[46] S.-S. Bao, X. Gong, H.-L. Li, S.-Y. Li, and Z.-G. Si, Phys. Rev. D **85**, 075005 (2012).